Experimental and Numerical Investigations for an Advanced Modeling of Two-Phase Flow and Mass Transfer on Column Trays

Dr.-Ing. Vineet Vishwakarma, TU Dresden (Germany)

1. Summary

Distillation is the leading thermal separation technology that is carried out in millions of tray columns operating globally.[1] Despite being the biggest energy consumers and the largest single investments in separation industry, these columns will remain in service in the future due to unavailability of any industrially viable alternative.[2] However, rising energy costs and alarming emergency to reduce greenhouse gas emissions demand urgent improvement in the energy efficiency of separation processes globally. My PhD thesis proposes that the energy efficiency of distillation columns can be improved by tuning the dynamics of the evolving two-phase dispersion based on design modification and revamping for maximum tray and column efficiencies. Therefore, it becomes inherently necessary to understand how the two phases evolve over the trays and how they link to the tray and column efficiencies for the given tray designs, systems and operating conditions. Only then, the cost and energy savings and reduction in their global carbon footprint can be achieved by strategically iterating the tray design and revamp with respect to the resulting tray and column efficiencies (see **Fig. 1**). Realizing the proposed strategy urges for significant advancement in the efficiency modeling approaches, which was the objective of my thesis. Validation of the advanced efficiency model calls for further innovations in flow imaging and efficiency measurement techniques, which were achieved in this thesis too.

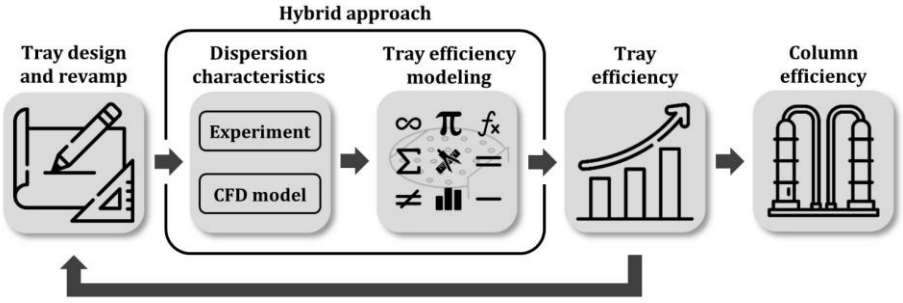

Figure 1. Strategy for improving column tray efficiency.

2. State of the art

2.1. Tray efficiency models: The fashion in which the two phases flow in the complex dispersion volume on the tray has strong influence on the tray efficiency. Numerous studies (later reviewed in this abstract) have revealed the existence of gross liquid flow maldistribution on the trays, which prompted the development of mathematical models accounting for the impact of liquid maldistribution on the tray efficiency. Such models are based on the relationships developed from the analyses of two-phase flow, crossflow hydraulics, and mass transfer over the trays,[3] and are categorized here. The first category comprises of basic tray models that consider perfectly mixed and plug flow of liquid on a tray.[4] The second category includes the pool models considering liquid mixing through perfectly mixed stages along the flow path length.[5,6] The diffusional models form the third category, where liquid mixing is included via eddy diffusion mechanism.[7-9] The next category comprises of the non-uniform flow model, which analyzes the effect of non-uniform liquid flow profiles (in the absence of liquid mixing) on the tray efficiency.[10] Lastly, the residence time distribution (RTD) model

describes the flow and mixing patterns through liquid RTD function ($f(t)$) and evaluates their effect on the tray efficiency.[11] A three-dimensional categorization of these models based on tray resolution (i.e., in terms of mathematical segmentation), liquid mixing and flow fields is presented in **Fig. 2**. This classification allows an easy interpretation of the model categories. Some models consider the whole tray as one unit, whereas some segment the tray into channels and cells (or pools) for material balancing. Flow patterns in terms of velocities and stream functions are also incorporated in few models. The degree of liquid mixing on a tray is specified on the third axis. An appropriate model should take the realistic liquid mixing into account, and hence, must lie between the extreme points of that axis. Moreover, an ideal model would be the one that incorporates flow and mixing patterns at the best possible resolution to predict the tray efficiency accurately.

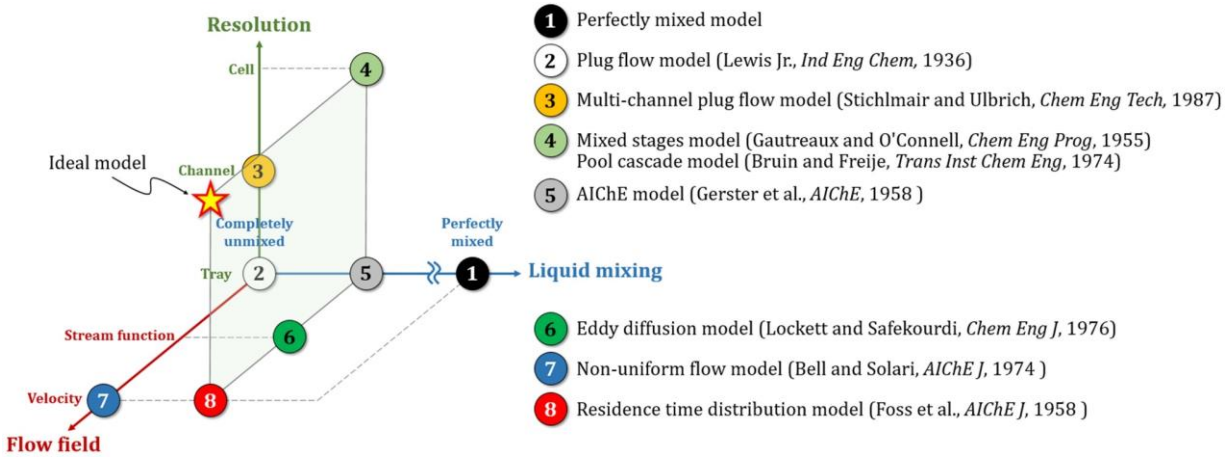

Figure 2. Graphical categorization of the conventional tray efficiency models.

2.2. Flow imaging techniques: Accurate flow visualization on industrial-scale column trays is challenging because of the chaotic and three-dimensional nature of two-phase crossflow. Full hydrodynamic data corresponds to the distributions of effective froth height, liquid holdup and RTD parameters over an entire tray. γ-ray densitometry technique[12] has been used to determine liquid holdup at selective locations on small trays and in rectangular columns. The application of γ-ray computed tomography in circular tray columns has been limited to process monitoring and troubleshooting.[13] Furthermore, liquid maldistribution (with respect to a desirable uniform and unidirectional flow) has been identified via measurements of RTD and velocity patterns.[14] Such information is usually retrieved from the two-phase dispersion above the tray through flow monitoring of a liquid tracer using camera techniques (photographic[8] and infrared[15]) and (multiple) point measurements (fiber-optic probes,[16] conductivity probes,[17] and wire-mesh sensor[18]). Other studies relying on point measurements used thermocouples,[19] strain gauge probes,[20] thermometers,[21] and hot film anemometer.[22]

2.3 Chemical systems for efficiency measurement: For validating model predictions based on hydrodynamic data, the tray and points efficiency measurement are required at same operating conditions. Achieving this requires complex chemical systems, experimental setups (e.g., semi-industrial distillation facilities, mockups with gas conditioning, recirculation and treatment) and analytics (e.g., gas-liquid chromatography). For this purpose, the chemical systems used in the literature comprise of organic distillation systems,[23] gas stripping systems,[24] gas absorption systems[25] and air humidification systems.[26] Further specifications of each system category is available in my PhD thesis.

2.4. Approaches for column efficiency estimation: The column efficiency is the ratio of number of equilibrium stages and number of actual trays in a column. This efficiency implies how big an actual column would be for the targeted component specification. Therefore, it is crucial to understand how the individual tray

efficiencies affect the number of trays in a column. In this context, only three methods exist in the literature - O'Connell's correlation,[27] Lewis Jr.'s analytical method[4] and Mathias' graphical method.[28]

3. Problems addressed

3.1. Black box evaluation of tray efficiency: The conventional models depend on liquid-side parameters (such as Péclet number, number of perfectly mixed pools, and so forth) that are determined by tracer sampling only at the tray outlet. This implies that these models consider homogeneous flow of liquid represented by the given parameters. In reality, liquid flow characteristics can vary over the tray area, because of the agitation caused by rising vapor, expanding and contracting flow path, and so on. However, these models are incapable of utilizing local tracer data at different tray locations. Such evaluation of the tray efficiency points to the general perception of distillation trays as a black box.

3.2. No consideration to vapor maldistribution: The existing models only consider uniform vapor flow through the trays and ignore any vapor maldistribution. Liquid hydraulic gradients on a tray can cause non-uniform vapor distribution, and vice-versa.[29] Only three studies[29-31] are known to extend the eddy diffusion concept for predicting tray efficiency based on vapor maldistribution, but they only considered perfectly mixed and plug flow of liquid on the tray. Even for these theoretical cases, their predictions contradicted each other. This demands further investigation on the influence of vapor maldistribution on the tray efficiency.

3.3. Unavailability of a versatile flow imaging technique: Different imaging techniques are required for quantifying effective froth height, liquid holdup and RTD. γ-ray densitometry can only reveal liquid holdup profiles at selective tray locations. Estimation of the effective froth height by Lockett et al.[25] is the only approach available in the literature, where the visually estimated height corresponds to the liquid holdup of 10% in a rectangular tray column. A verification of Lockett et al. criterion is still pending (even for the circular columns), whereas the froth height distribution over the entire tray area remains unavailable. Although previous imaging techniques were successful in identifying gross liquid maldistribution, the camera techniques can provide flow patterns near the dispersion surface only, whereas the point measurements suffer from a variety of challenges such as high intrusiveness, low spatial resolution, complex calibration scheme, to name only a few. Thus, the existing experimental studies lack a complete 3D hydrodynamic description of an operational industrial-scale distillation tray.

3.4. Complexities of efficiency measurements: The existing chemical systems have numerous operational and technical limitations and safety concerns. For example, organic distillation systems require industrial facilities such as pressure vessel, condenser and reboiler to process hazardous substances. Gas stripping systems require gas dissolution in the liquid, which makes them suitable for trays with low liquid residence time only. Gas absorption systems pose health and safety concerns, because of the application of gases such as NH_3, CO_2, and SO_2, and hence require effluent gas recirculation and treatment. The air conditioning systems require precise conditioning of air prior to column inlet, which is rather challenging to control. Furthermore, point efficiency are commonly measured in small-scale Oldershaw columns, although the flow conditions in such columns vary considerable from that in large-scale facilities.

3.5. Rudimentary estimation of column efficiency: The existing approaches for column efficiency prediction do not consider the variations in individual tray efficiencies governed by two-phase flow and mixing profiles and VLE characteristics of the mixtures. O'Connell's correlation ignores any description of tray efficiency and can only provide conservative estimations. The analytical and graphical methods assign a fixed tray efficiency and VLE slope to each tray in a column and accordingly calculate the column efficiency. These generalizations confirm that the existing methods are only applicable for qualitative estimation of column efficiency.

4. Key innovations

4.1 Advanced tray efficiency model: As the RTD model (**Fig. 3a**) was recognized as the most realistic among the conventional models, it was subjected to further refinement in my thesis. The derivation of the new model (called the refined RTD (RRTD) model) starts with geometrical division of a tray into an arbitrary number of compartments along the flow path length as shown in **Fig. 3b**.

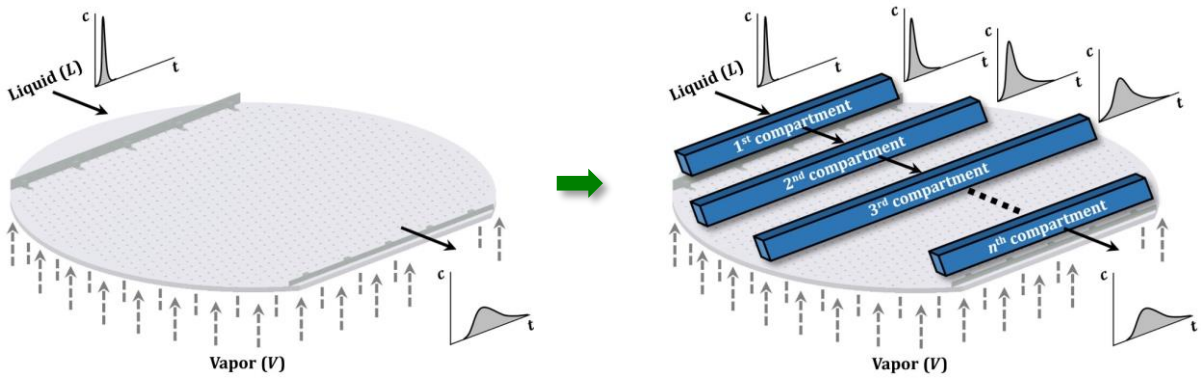

(a) (b)

$$E_{\mathrm{MV}} = \frac{1-\int_0^{\infty} \exp(-\lambda E_{\mathrm{OV}} t/\tau)\cdot f(t)\mathrm{d}t}{\lambda \int_0^{\infty} \exp(-\lambda E_{\mathrm{OV}} t/\tau)\cdot f(t)\mathrm{d}t} \quad \text{(Eq. 1)}$$

$$E_{\mathrm{MV}} = \frac{1}{\lambda}\left[\left\{\prod_{i=1}^{n}\left(1 + a_i d_i \lambda E_{\mathrm{MV,i}}\right)\right\} - 1\right] \quad \text{(Eq. 2)}$$

Figure 3. (a) Schematic representation of the standard RTD model, and (b) the new refined RTD (RRTD) model including tracer concentration (c-t) charts and respective mathematical formulations. (E_{MV} – tray efficiency, E_{OV} – point efficiency, $f(t)$ – liquid RTD function, t – time variable, τ – liquid mean residence time and λ – stripping factor).

In **Fig. 3b**, the tray is partitioned into n compartments that are separated from each other by the boundaries referred to as dividers. The liquid flows serially through the compartments, while the vapor flows through them normal to the tray deck. It is assumed that each compartment behaves like a single-pass crossflow tray with distinct RTD and Murphree efficiency according to the RTD model. The assumptions involved in the new model derivation can be found in my thesis. Each compartment (index i) has a unique RTD function $f_i(t)$ and compartment efficiency $E_{\mathrm{MV},i}$. Similar to the RTD model, constant flow of liquid (L) is considered in the compartments, so that $Lf_i(t)dt$ can represent the liquid streams exiting the i^{th} compartment between time t and $t + dt$. The overall vapor flow (V) is considered to be divided between n compartments as $V_i = a_i d_i V$ such that $\sum_{i=1}^{n} a_i = 1, \sum_{i=1}^{n} d_i = n,$ and $\sum_{i=1}^{n}(a_i \cdot d_i) = 1$. Here, a_i and d_i are the area fraction and vapor allocation index of the i^{th} compartment, respectively for $i = 1, 2, \ldots n$. This index is unity in each compartment for uniform vapor distribution, whereas any other distribution of this index in the compartments would represent vapor maldistribution over the tray. Further, the stripping factor for the i^{th} compartment can be defined as $\lambda_i = mV/L = a_i d_i \lambda$, where m is the slope of vapor-liquid equilibrium (VLE) line. Since point efficiency is a weak function of the superficial vapor velocity,[15] it can be assumed as constant over the tray regardless of any vapor maldistribution. Accordingly, the efficiency $\left(E_{\mathrm{MV},i}\right)$ of the i^{th} compartment via material balancing similar to Eq. 1 is

$$\frac{1}{1 + \lambda_i E_{\mathrm{MV},i}} = \int_0^{\infty} e^{-\frac{\lambda_i E_{\mathrm{OV}} t}{\tau_i}} \cdot f_i(t)dt\,. \quad \text{(Eq. 3)}$$

τ_i is the mean liquid residence time in the i^{th} compartment, which can be written as $\tau_i = b_i\tau$ such that $\sum_{i=1}^{n} b_i = 1$. Using these and previous simplifications in Eq. 3 provides

$$\frac{1}{1 + a_i d_i \lambda E_{\mathrm{MV},i}} = \int_0^\infty e^{-\frac{a_i d_i \lambda E_{\mathrm{OV}} t}{b_i \tau}} f_i(t)dt = \mathcal{F}_i\left(\frac{a_i d_i \lambda E_{\mathrm{OV}}}{b_i \tau}\right), \qquad \text{(Eq. 4)}$$

where $\mathcal{F}_i$ is the Laplace transform of $f_i(t)$. The system theory[32] relates the RTD functions of the tray and compartment as

$$f(t) = f_1(t) \otimes f_2(t) \otimes \cdots f_n(t)\,. \qquad \text{(Eq. 5)}$$

The symbol $\otimes$ represents the convolution integral. Transforming Eq. 5 and substituting the Laplace functions from Eqs. 1 and 4 in Eq. 5 (as explained in my thesis) leads to the new RRTD model as

$$E_{\mathrm{MV}} = \frac{1}{\lambda}\left[\left\{\prod_{i=1}^{n}\left(1 + a_i d_i \lambda E_{\mathrm{MV,i}}\right)\right\} - 1\right]. \qquad \text{(Eq. 2 (see Fig. 3))}$$

For the first time, the tray efficiency (according to the new RRTD model) can account for the variations in the local two-phase fluid dynamics via local liquid RTD functions and vapor allocation indices of the compartments. Mathematically, the RRTD model was validated by verifying its predictions for perfectly mixed flow and plug flow of liquid on the tray. Details regarding mathematical validation of the RRTD model are available in my thesis. For experimental validation of this model, a comprehensive hydrodynamic and mass transfer description specific to the two-phase dispersion in an industrial-scale tray column is indispensable.

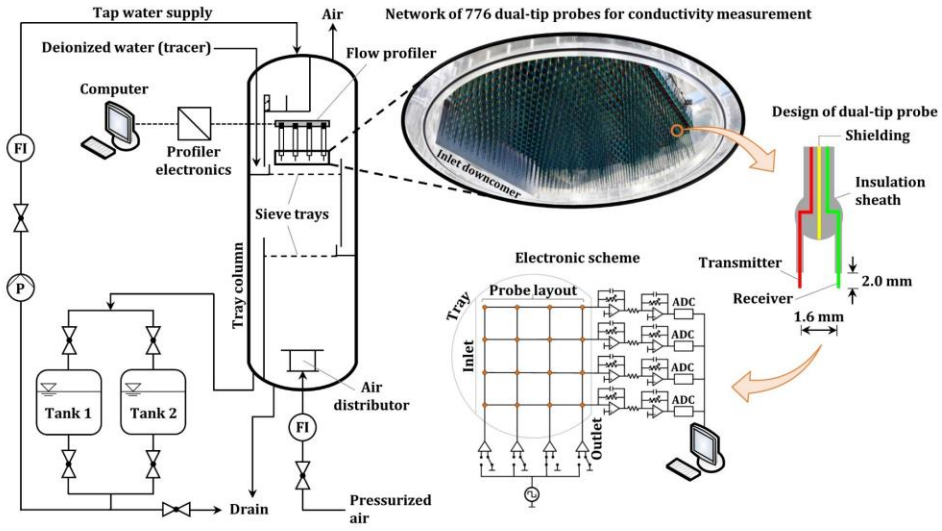

Figure 4. Multiplex flow profiler installed in the DN800 column facility (including probe details and electronic scheme exemplarily shown for a 4 x 4 arrangement).

4.2. Novel multiplex flow profiler: For unified hydrodynamic characterization, the new multiplex flow profiler comprising of a skeletal grid of 28 × 32 headers holding 776 dual-tip conductivity probes was developed and patented (see **Fig. 4**).[33] Each probe was connected to the profiler electronics via header grid as exemplarily shown for a 4 × 4 grid in the electronic scheme in **Fig. 4**. The probes uniformly span over the tray area with high spatial resolution of 21 mm × 24 mm. Each probe was a multi-layer printed circuit board housing three separate electrodes namely transmitter, receiver and shielding in an insulating sheath enclosure. Such probe

configuration eliminated cross talk and simplified calibration and data processing schemes. Only the tips of transmitter and receiver electrodes were exposed to the two-phase flow, which points to low invasiveness of the profiler. As illustrated in **Fig. 4**, an excitation voltage was applied to each header (parallel to the weir) sequentially via multiplexing scheme, which activated the corresponding transmitter electrodes. Parallel sampling of all longitudinal headers returned signals from all probe receivers based on the local instantaneous conductance near the probe tips. This way, each probe measured the temporal variation of the presence of liquid and gas locally. The probes also identified the local variation in the liquid conductivity owing to tracer injection. These capabilities of the profiler refer to its versatility regarding hydrodynamic quantification. The acquired signals were appropriately amplified and digitized into a 3D data matrix of size $32 \times 28 \times n$ for post-processing. Here, n is the product of the total measurement time and the sampling frequency (= 5000 Hz). Based on this procedure, the two-phase planar data were gathered by the profiler at multiple elevations above the tray deck via vertical adjustments for 3D measurements.

4.3. New analytical approach for measuring effective froth height: In my thesis, a new approach was proposed for determining effective froth height distribution based on profiler data gathered at multiple elevations above the tray. In that approach, the response of each probe was analyzed based on field distribution governed by local phase continuity, geometry factor, and inter-probe interaction. Because of their varying dispersion characteristics, the probe responses varied with the regions as simplified in **Fig. 5**. The slope of the probe data above a certain threshold (i.e., liquid-only response (L_1) acted as a region discriminator and followed an s-shaped trend in **Fig. 5**. The local effective froth height was the one, where the slope value approached zero. This led to 3D distribution of effective froth height for the first time, which is again crucial for quantifying realistic 3D liquid holdup and flow profiles on the tray.

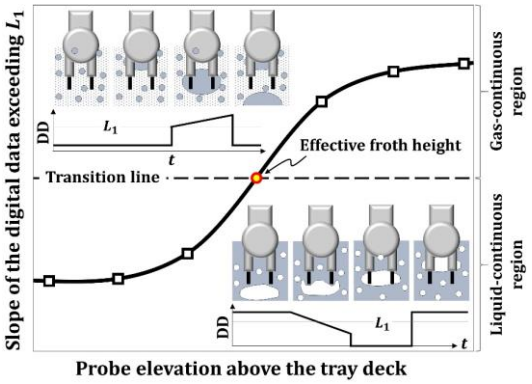

Figure 5. Simplified probe responses for estimating effective froth height based on the overall slope of the probe signals exceeding liquid-only (L_1) response (DD stands for digital data).

4.4. New chemical system for direct efficiency measurement: In my thesis, I have proposed the air-led stripping of isobutyl acetate from aqueous solution for direct measurement of tray and point efficiencies on distillation trays. The new system posed no health and safety hazards due to very low concentration of isobutyl acetate in the effluent gas stream (according to EU standard), and was easy to implement on large air-water mockup facility without any major modification. Only an extra pump for batch preparation and nine sampling taps over the trays were sufficient for the facility modification. This system was suitable for large trays with low liquid residence times, whereas mixing of isobutyl acetate with liquid for initial batch preparation was much easier than gas dissolution in conventional systems. The liquid properties remained unchanged after the addition of isobutyl acetate. Fast and well-accepted UV-spectroscopy of liquid samples for

concentration measurements made the application of the new system highly convenient. Based on concentration data, the tray and point efficiencies and the stripping factor were calculated as discussed in my thesis.

4.5. Novel strategy for column efficiency calculation: My thesis proposed a new strategy for evaluating column efficiency based on two-phase flow and mixing profiles on individual trays and VLE data of binary mixtures. In that strategy, an appropriate thermodynamic model was employed for generating VLE data of binary mixtures. Processing the flow and mixing profiles with the VLE data using a novel iterative approach and tray efficiency model led to the slope of the VLE line and tray efficiency. Following this approach for each tray allows exclusive inclusion of individual tray efficiencies (varying from tray to tray) in the calculation of column efficiency for the first time. Thus, a priori estimation of the column performance in the design phase is possible now. This is fortuitous for the separation industry as sometimes the potential areas for efficiency improvements are only revealed in the post design phase leading to considerable cost and energy losses.

5. Application, implementation and results

5.1. Hydrodynamic characterization of an operational tray: This section presents the measured hydrodynamic data corresponding to a sieve tray subjected to multiple gas and liquid loadings. The evidences regarding excellent reproducibility of the data presented in this entire abstract can be found in my thesis. First, using the single-threshold technique (based on separate γ-ray CT measurements),[34] the time-averaged liquid holdup (α) distribution at different profiler elevations above the tray were obtained as exemplarily shown in **Fig. 6**. In this figure, each black pixel shows holdup masking that means the probe elevation was beyond the local effective froth height (obtained via new procedure discussed in section 4.3). The mean effective froth height for the two-phase dispersion in **Fig. 6** was 57 mm. In this figure, the liquid holdup increases with the profiler elevation with the highest holdup appearing near the mean effective froth height, because of the liquid suspension by gas jets from the lower elevation. Beyond the effective froth height, the liquid holdup drastically reduces to zero. Further, Lockett et al.[25] criterion suggested that the mean effective froth height corresponds to the height, where the average liquid holdup is 10%. Based on **Fig. 6**, the criterion predicts the mean effective froth height as 60 mm, which is reasonably accurate with respect to the measured height (i.e., 57 mm). This investigation confirms the validity of Lockett et al. criterion for froth height estimation in large circular columns. Since majority of the probes were within the liquid-continuous froth with reasonable holdup homogeneity at 40 mm elevation, the profiler was placed at this elevation for performing tracer-based experiments regarding flow visualization.

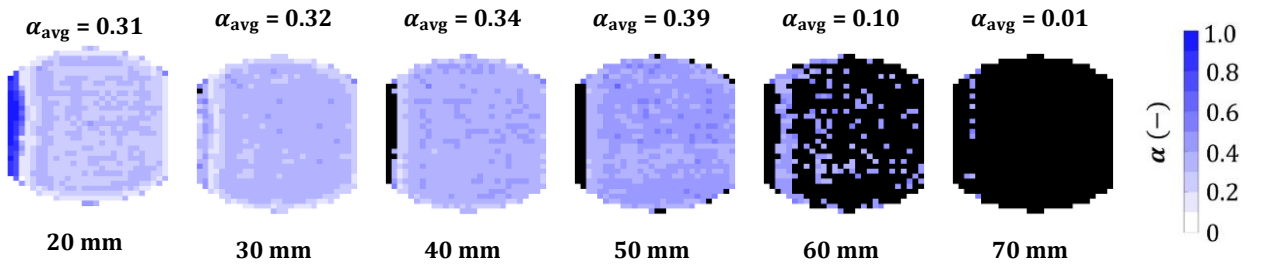

Figure 6. Liquid holdup (α) distribution (including average holdup values) at given elevations above the tray for the loadings 4.30 $m^3m^{-1}h^{-1}$ and 1.77 $Pa^{0.5}$ (black pixels – holdup masking for the probes, whose elevation exceed their local effective froth height).

At 40 mm elevation, the profiler probes monitored the liquid flow over the tray by injecting tracer before inlet weir (see **Fig. 4**). Based on the processed profiler data, the flow and mixing patterns are shown via distributions of mean appearance time ($\tilde{\tau}$) and variance ($\tilde{\sigma}^2$) in **Fig. 7**a and b, respectively. The isocontours of

these parameters are also superimposed on these figures. The unidirectional liquid velocities over the tray are depicted in **Fig. 7**c. **Fig. 7** exhibits a reasonable symmetry in the liquid flow and mixing characteristics with respect to tray centerline. The liquid backup in the downcomer is pushed towards the centerline by the wall curvature causing a parabolic velocity distribution (with peak velocities along the centerline) after the tray inlet (see Figure **7**c). Consequently, lower mean appearance times and variances appear over the tray area with higher liquid velocities in the parabolic distribution. Further along the flow path length, the velocities over the majority of the tray deck homogenize, because of the gas flow resistance and agitation causing a systematic rise in mean appearance time and variance over that tray area.

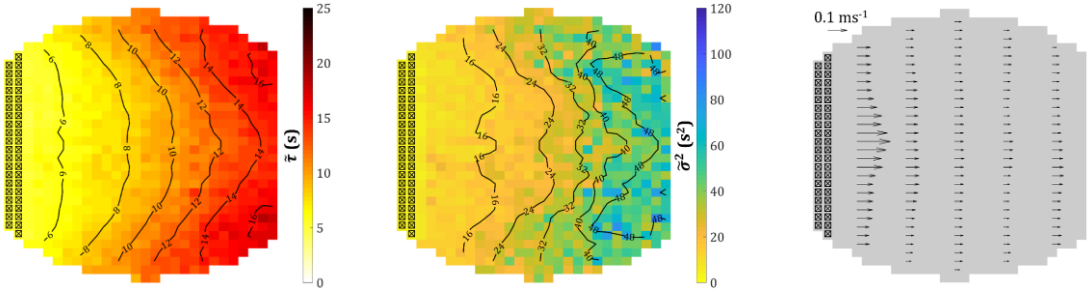

Figure 7. Distributions of (a) mean appearance time, (b) variance, and (c) unidirectional liquid velocity for the loadings 4.30 $m^3m^{-1}h^{-1}$ and 1.77 $Pa^{0.5}$ (note - first two probe columns are disregarded for being above the local effective froth heights).

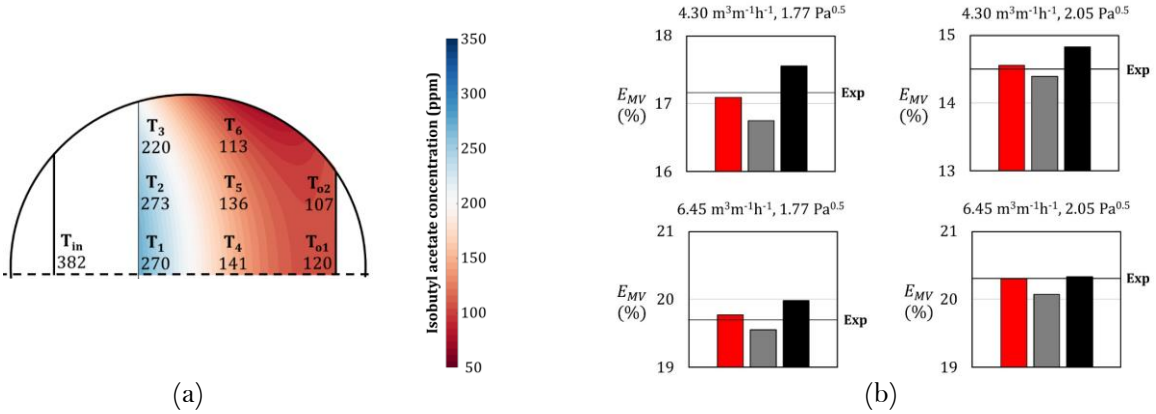

Figure 8. (a) Liquid concentrations (in ppm) at tap locations superimposed over the spatial concentration distribution on the reduced tray for the tray loadings 4.30 $m^3m^{-1}h^{-1}$ and 1.77 $Pa^{0.5}$, and (b) tray efficiencies for all operating conditions that were measured and predicted by the new RRTD model (■), standard RTD model (■) and AIChE model (■), see **Fig. 2**).

***5.2.* Model validation and efficiency measurements:** For RRTD model application, the tray was geometrically partitioned into three compartments for obtaining the RTD function (using axial dispersion model (ADM)) for each compartment based on hydrodynamic data. The flow conditions in the first compartment violated some of the assumptions of the ADM. As a result, the reduced tray comprising of two compartments was considered and the hydrodynamic data was accordingly averaged for the RRTD model application. Further, the concentration distribution of isobutyl acetate over the reduced tray is shown in **Fig. 8**a. The taps T1 and T2 have similar concentrations because of the uniform liquid appearance time and very high liquid mixing there (refer to **Fig. 7**). The liquid spent slightly longer near the column wall causing lower species

concentration at tap T3 compared to T1 and T2. Along the taps T4–T6, a variation in the species concentration persists according to the gradient in the mean appearance time. Similar concentrations for the taps To1 and To2 were recorded, because of the similar liquid appearance time and reduced driving force for species transfer to the gas. From the concentration data, the point and tray efficiency and stripping factor were calculated for model validation. For simplicity, only measured tray efficiencies are displayed in **Fig. 8**b. The predictions based on hydrodynamic data from the RRTD model, RTD model and AIChE model are compared in **Fig. 8**b too. Very high liquid backmixing, low liquid diffusivity, uniform liquid velocities (see **Fig. 7**c) and uniform vapor distribution led to only small distinctions in the model predictions. Even for the given data, the RRTD model is the most accurate as its efficiency predictions are closest to the measured efficiencies. The RTD model and the AIChE model predictions are lower and higher than the measured efficiencies and are less accurate. Further promise of the RRTD model is graphically demonstrated via case studies in **Fig. 9**.

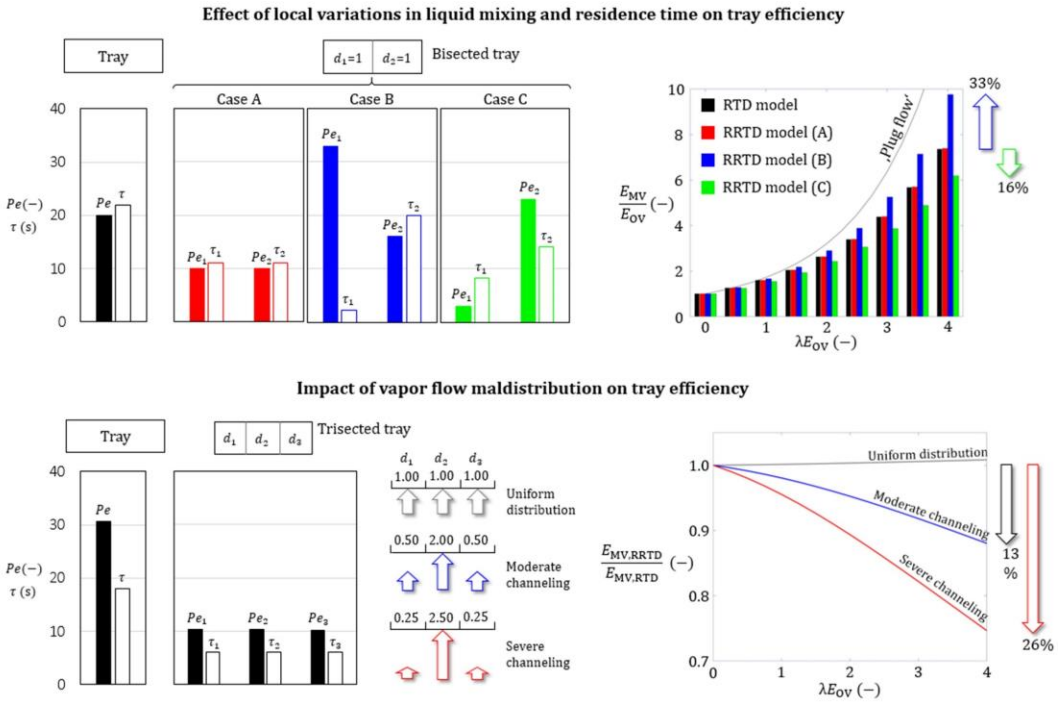

Figure 9. Case studies showing that the RRTD model can account for local variations in the liquid flow (breaking black box convention) and vapor maldistribution unlike the standard RTD model (Pe – Péclet no., τ – mean residence time).

5.3. Realistic estimation of column efficiency: In another case study in my thesis, the column efficiencies were calculated (based on the strategy proposed in section 4.5) for different degrees of liquid backmixing on the trays, varying VLE data (of 15 commercial mixtures) and different point efficiencies. **Fig. 10** summarizes those efficiencies at a fixed point efficiency for three cases of liquid backmixing (severe, intermediate, and lowest). Accordingly, the column efficiencies are the highest for the lowest backmixing, and vice-versa. For each case, the tray efficiency varied from tray to tray owing to variation in the VLE data (not shown here) making this method much more accurate than the conventional approaches. Further, binary mixtures with high relative volatilities are easy to separate via distillation, and hence require less number of trays in the column. However, this is only valid when the column trays operate with low liquid backmixing and high point efficiency. Otherwise, higher number of trays are needed for the targeted separation, thereby deteriorating the overall column efficiency (refer to mixtures with high relative volatility in **Fig. 10**).

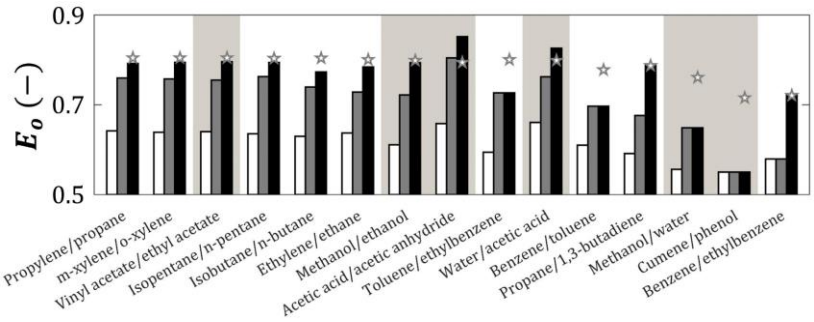

Figure 10. Predictions of column efficiency (E_O) for different binary mixtures (cases of liquid backmixing: severe (Pe =2): white, intermediate (Pe =10): gray, low (Pe =36): black, and stars indicate the lowest back-mixing case for hypothetical mixtures with constant relative volatility).

6. References

1. Sholl DS, Lively RP. Seven chemical separations to change the world. *Nature News*. 2016;532(7600):435.
2. Olujić Ž, Kaibel B, Jansen H, Rietfort T, Zich E, Frey G. Distillation column internals/configurations for process intensification. *Chem Biochem Eng* 2003;17:301-309.
3. Luo N, Qian F, Ye Z-C, Cheng H, Zhong W-M. Estimation of mass-transfer efficiency for industrial distillation columns. *Ind Eng Chem Res*. 2012;51(7):3023-3031.
4. Lewis Jr WK. Rectification of binary mixtures. *Ind Eng Chem*. 1936;28(4):399-402.
5. Gautreaux MF, O'Connell HE. Effect of length of liquid path on plate efficiency. *Chem Eng Prog*. 1955;51(5):232-237.
6. Bruin S, Freije A. A simple liquid mixing model for distillation plates with stagnant zones. *Trans Inst Chem Eng*. 1974;52(1):75-79.
7. Gerster JA, Hill AB, Hochgraf NN, Robinson DG. *Tray Efficiencies in Distillation Columns- Final Report from the University of Delaware*. American Institute of Chemical Engineers;1958.
8. Porter KE, Lockett MJ, Lim CT. The effect of liquid channeling on distillation plate efficiency. *Trans Inst Chem Eng*. 1972;50(2):91-101.
9. Lockett MJ, Safekourdi A. The effect of the liquid flow pattern on distillation plate efficiency. *Chem Eng J*. 1976;11(2):111-121.
10. Bell RL, Solari RB. Effect of nonuniform velocity fields and retrograde flow on distillation tray efficiency. *AlChE J*. 1974;20(4):688-695.
11. Foss AS, Gerster JA, Pigford RL. Effect of liquid mixing on the performance of bubble trays. *AIChE J*. 1958;4(2):231-239.
12. Hofhuis PAM. *Flow regimes on sieve-trays for gas/liquid contacting*, Technische Hogeschool Delft; 1980.
13. Haraguchi MI, Calvo WAP, Kim HY. Tomographic 2-D gamma scanning for industrial process troubleshooting. *Flow Meas Instrum*. 2018;62:235-245.
14. Bell RL. Residence time and fluid mixing on commercial scale sieve trays. *AIChE Journal*. 1972;18(3):498-505.
15. Li Y, Wang L, Yao K. New technique for measuring fluid flow patterns on a multiple downcomer tray. *Ind Eng Chem Res*. 2007;46(9):2892-2897.
16. Solari RB, Bell RL. Fluid flow patterns and velocity distribution on commercial-scale sieve trays. *AIChE J*. 1986;32(4):640-649.
17. Yu KT, Huang J, Li JL, Song HH. Two-dimensional flow and eddy diffusion on a sieve tray. *Chem Eng Sci*. 1990;45(9):2901-2906.
18. Schubert M, Piechotta M, Beyer M, Schleicher E, Hampel U, Paschold J. An imaging technique for characterization of fluid flow pattern on industrial-scale column sieve trays. *Chem Eng Res Des*. 2016;111:138-146.
19. Stichlmair J, Ulbrich S. Liquid channelling on trays and its effect on plate efficiency. *Chem Eng Technol*. 1987;10(1):33-37.
20. Biddulph MW, Bultitude DP. Flow characteristics of a small-hole sieve tray. *AIChE J*. 1990;36(12):1913-1916.
21. Porter KE, Yu KT, Chambers S, Zhang MQ. Flow patterns and temperature profiles on a 2.44 m diameter sieve tray. *Chem Eng Res Des*. 1992;70(A):489-500.
22. Liu C, Yuan X, Yu KT, Zhu X. A fluid–dynamic model for flow pattern on a distillation tray. *Chem Eng Sci*. 2000;55(12):2287-2294.
23. Yanagi T, Sakata M. Performance of a commercial scale 14% hole area sieve tray. *Ind Eng Chem Process Des Dev*. 1982;21(4):712-717.
24. Johnson A, Marangozis J. Mixing studies on a perforated distillation plate. *The Canadian Journal of Chemical Engineering*. 1958;36(4):161-168.
25. Lockett MJ, Kirkpatrick RD, Uddin MS. Froth regime point efficiency for gas-film controlled mass transfer on a two-dimensional sieve tray. *Trans Inst Chem Eng*. 1979;57(1):25-34.
26. Lamprecht JH. *The development of simplistic and cost-effective methods for the evaluation of tray and packed column efficiencies*, Stellenbosch: Stellenbosch University; 2017.
27. O'connell H. Plate efficiency of fractionating columns and absorbers. *Trans AIChE*. 1946;42:741-755.
28. Mathias PM. Visualizing the McCabe-Thiele diagram. *Chem Eng Prog*. 2009;105(12):36-44.
29. Mohan T, Rao KK, Rao DP. Effect of vapor maldistribution on tray efficiency. *Ind Eng Chem Process Des Dev*. 1983;22(3):376-380.
30. Furzer I. The effect of vapor distribution on distillation plate efficiencies. *AIChE Journal*. 1969;15(2):235-239.
31. Lockett MM, Dhulesia HA. Murphree plate efficiency with nonuniform vapour distribution. *Chem Eng J*. 1980;19(3):183-188.
32. Levenspiel O. *Chemical reaction engineering*. 3rd ed: John Wiley and Sons; 1999.
33. Vishwakarma V, Schleicher E, Schubert M, Tschofen M, Löschau M, Inventors; Helmholtz Zentrum Dresden Rossendorf eV, assignee. Sensor zur Vermessung von Strömungsprofilen in großen Kolonnen und Apparaten. US patent DE1020181245012020.
34. Vishwakarma V, Schleicher E, Bieberle A, Schubert M, Hampel U. Advanced flow profiler for two-phase flow imaging on distillation trays. *Chem Eng Sci*. 2021;231.